Journal of Materials Chemistry A

Accepted Manuscript

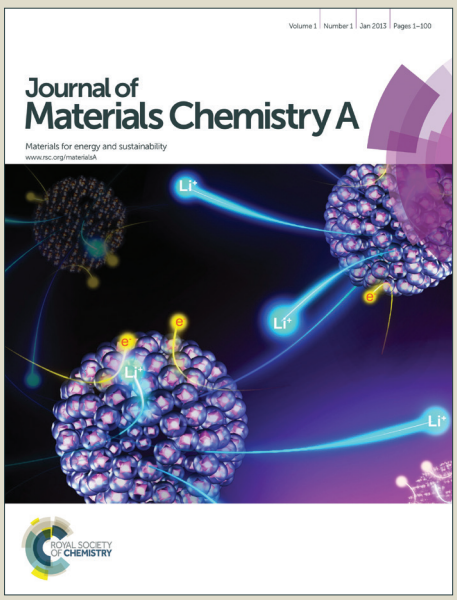

ROYAL SOCIETY OF CHEMISTRY

www.rsc.org/materialsA

Journal Name

ARTICLE

A-site deficient chromite perovskite with *in-situ* exsolution of nano Fe : A promising bi-functional catalyst bridging growth of CNTs and SOFCs

Received 00th January 20xx,
Accepted 00th January 20xx

DOI: 10.1039/x0xx00000x

www.rsc.org/

Yi-Fei Sun,[a] Jian-Hui Li,[b,c*] Meng-Ni Wang,[a] Bin Hua,[a,d] Jian Li,[d] and Jing-Li Luo[a,*]

For the first time, an iron doped lanthanum strontium chromite with A-site deficiency (A-LSCFe) was fabricated and utilized as an effective bi-functional catalyst for the growth of multiple-walls carbon nanotubes (MWCNTs) and solid oxide fuel cells (SOFCs). The introduction of A-site deficiency significantly facilitates the in-situ exsolution of nano iron particles on which considerable amount of MWCNTs are grown. The material was also used as the anode catalyst for SOFCs and proved to be very effective anode catalyst in comparison with stoichiometric material (sto-LSCFe). The exsolved nano iron particles on A-LSCFe provide much more active sites for the oxidation reaction of fuel, leading to sharp enhancement of the electrochemical performance of the cell. It is also discovered that the growth of MWCNTs with high electron conductivity leads to a further improvement on the electricity output.

Introduction

The development of advanced devices that enhance the efficiency of fuel utilization has been a research focus for the scientists worldwide in light of the impact of potential energy crisis. The solid oxide fuel cells (SOFCs) have been regarded as one of the most promising technologies which can continuously produce electricity as long as the fuel inputs are supplied. For the SOFCs fed with hydrocarbon such as methane, the fuel usually decomposes, at elevated temperature, to form amorphous carbon species which degrade the catalytic activity by blocking the active sites.[1] To overcome this challenge, the modification of anode[2] and the addition of vapor to hydrocarbons[3] are the two main methods to mitigate the negative influence of coking.

In recent years, the carbon nanotubes (CNTs) have drawn increasing attention since they were found to be able to significantly enhance the performance of various energy storage systems including super capacitor[4] and fuel cells.[5] In addition, the CNTs also exhibit attractive properties of high thermal conductivity and superior electrical conductivity, which accelerate the heat transfer and increase the reaction rate during the electrochemical reactions.[6,7]

The catalytic chemical vapor deposition (CCVD) is the most widely accepted CNTs growth technology, in which a variety of active metals such as Ni, Fe, and Co[8, 9] as well as some of their corresponding alloy[10] play the role of being the localized growth sites for the prepared CNTs. Two steps involved in the process of CCVD consist of formation of active nanoparticles and the introduction of carbon sources. It was also revealed that the dimension parameters of CNTs are controlled by the size and distribution of metallic particles.[11, 12] In-situ exsolution of metallic nano particle on perovskite[13] is regarded as a time-efficient and effective way to generate well-dispersed metallic particles compared to traditional impregnation method. However, the exsolution amount was strongly restricted by the stoichiometric composition of perovskite. Recent research on A-site deficient perovskite found that the alternation of ratio of A/B can obviously facilitate the in-situ exsolution of well-dispersed metallic particles with uniform particle sizes[14] Consequently, the A-site deficient perovskite with uniform metallic particles anchored on could be seen as a promising alternative catalyst enabling the growth tailored CNTs. However, to our best knowledge, no report on the A-site deficient perovskite with exsolution of nano particle for SOFC performance text has been shown so far.

So far, very limited information on the enhancing effect of MWCNTs on SOFCs has been reported. Only the addition of multiple-walls carbon nanotubes (MWCNTs) to $Pr_{0.6}Sr_{0.4}Fe_{0.8}Co_{0.2}O_3$ (PSFC) perovskite cathode material was revealed and it could control the size of nanoparticles, which reduced the area specific resistance of the material.[15] However, the fabrication process is complicated and time-consuming.

Herein, we report a novel fabrication method in which the iron doped lanthanum strontium chromite perovskite with A-site

[a] Department of Chemical and Materials Engineering, University of Alberta, Alberta, Canada, T6G 2V4. E-mail: jingli.luo@ualberta.ca.
[b] National Engineering Laboratory for Green Chemical Productions of Alcohols-Ethers-Esters, College of Chemistry and Chemical Engineering, Xiamen University, Xiamen, China, 361005. E-mail: jhli@xmu.edu.cn.
[c] Department of Chemistry and Applied Chemistry, Changji University, Changji, Xinjiang, China, 831100.
[d] School of Materials Science and Engineering, State Key Laboratory of Material Processing and Die & Mould Technology, Huazhong University of Science and Technology, Wuhan, China, 430074.

deficient (A-LSCFe) was used to *in-situ* exsolve nano particles on which considerable amount of MWCNTs are grown. The material thus fabricated was used as the anode catalyst for SOFC. The properties of the MWCNTs and the electrochemical performance of SOFCs were studied.

Experimental

Fabrication of electrode materials

The glycine nitrate combustion method was used to fabricate the $La_{0.7}Sr_{0.3}CrO_{3-y}$, $La_{0.7}Sr_{0.3}$ $Cr_{0.85}Fe_{0.15}O_{3-\xi}$ and $La_{0.6}Sr_{0.3}Cr_{0.85}Fe_{0.15}O_{3-\xi}$ anode materials for the fuel cell test, denoted as LSC, sto-LSCFe and A-LSCFe, respectively. Certain amounts of $La(NO_3)_2{\cdot}6H_2O$, $Sr(NO_3)_2$, $Fe(NO_3)_3{\cdot}9H_2O$, $Cr(NO_3)_3{\cdot}9H_2O$ and glycine were dissolved in deionized water firstly. The molar ratio of glycine to the total content of the metal cations was 2:1. The solution was stirred thoroughly and then heated on a hot plate at 500 ^{o}C until self-combustion started. The generated powders were ground and further calcined at 1300 ^{o}C in air for 3h to produce different anode materials. All the prepared materials and their corresponding denotation are shown in Table 1 below.

Table 1. Denotation of various materials

Compositions	Denotation
$La_{0.7}Sr_{0.3}CrO_{3-y}$	LSC
$La_{0.7}Sr_{0.3}$ $Cr_{0.85}Fe_{0.15}O_{3-\xi}$	Sto-LSCFe
$La_{0.6}Sr_{0.3}Cr_{0.85}Fe_{0.15}O_{3-\xi}$	A-LSCFe
Reduced $La_{0.6}Sr_{0.3}Cr_{0.85}Fe_{0.15}O_{3-\xi}$	Re-A-LSCFe
15mol% Fe impregnated in $La_{0.7}Sr_{0.3}CrO_{3-y}$	Fe/LSC

Fuel cell fabrication

Fuel cells were fabricated using commercial YSZ disks (FCM "fuelcellmaterials.com") as electrolyte with the thickness of 300 μm and diameter of 25 mm. The cathode was the mixture of equal weights of YSZ powder (TOSHO Company) and strontium doped lanthanum manganese (LSM). The anode was prepared through mixing equal weights of YSZ and prepared anode materials. Both cathode and anode inks were prepared from oxide powders dispersed in terpineol mixed with 10% polyethylene glycol (PEG) as screen printing binder. The electrode inks were deposited onto the YSZ electrolyte disc using screen printing to form a membrane electrode assembly (MEA) with the area of 1 cm^2, and then the cell was sintered at 1100 ^{o}C for 2h to form good binding between the electrodes and the electrolyte. The platinum paste and gold paste were painted on the cathode side and anode side, respectively, to serve as the current collectors.

Fuel cell test

Single cell tests were performed in a vertical furnace with a coaxial two-tube (inlet and outlet) set-up. The outlet tube was directly sealed (Ceramabond 503, Aremco Products) to the outer edge of the anode side of the single cell electrolyte to avoid leakage of fuel gas and oxygen. A Thermolyne F79300 tubular furnace was used to heat the cell. Hydrogen as the fuel was fed at a rate of 75 mL min^{-1}. The electrochemical performance of the fuel cell was measured using a Solartron 1287 instrument with 2588 frequencer. The polarization resistance of the cell was estimated based on the electrochemical impedance spectra (EIS) measured at the open circuit voltage with an AC potential signal of ±10 mV amplitude and the frequency range of 1 MHz to 0.1 Hz.

Materials characterization

The phase compositions of the synthesized powders were identified using a Rigaku Rotaflex X-ray diffractometer (XRD) with Cu Ka radiation, and the data were analyzed using JADE 5.0 software.

The micromorphology of the materials was determined by a JEOL 6301F scanning electron microscope (SEM). Additional information was gathered using an EOL JEM2100 transmission electron microscope (TEM) with an energy-dispersive X-ray spectroscopy (EDS) detector.

Hydrogen temperature programmed reduction (H_2-TPR) was performed using an AutoChem II 2920 instrument (Micromeritics, USA) equipped with a thermal conductivity detector (TCD). All samples were treated with helium at 1000^{o}C for 30 min before H_2-TPR. The flow rate for this analysis was 10% H_2/Ar at 10 mL min^{-1}, and the temperature ramping rate was 10 ^{o}C min^{-1}.

Thermogravimetric analysis (TGA) measurements were conducted using a TA Instruments SDT Q600 under 5% H_2/N_2 from 100^{o}C to 800^{o}C with a flow rate of 20 mL min^{-1} and a heating rate of 20 ^{o}C min^{-1}. The isothermal program of TGA was also conducted at targeted temperature with the gas flow rate of 20 ml min^{-1}.

Results and discussion

The crystallographic structure of the fresh and reduced compounds was examined by X-ray diffraction (XRD). The analysis of the data shows that both A-LSCFe, Sto-LSCFe as well as LSC materials exhibit perovskite-type structure and all main peaks are matched well with those of $LaCrO_3$ (JCPDS no.24-1016). Besides, no peak attributed to impurity was detected. The A-site deficient LSCFe was treated in 5%H_2-N_2 at 800 ^{o}C for 4h (denoted as Re-A-LSCFe) and the XRD pattern for corresponding material is also shown in Figure 1 (Re-A-LSCFe). It is found that the diffraction peak ascribed to metallic Fe could be detected, indicating the exsolution of metallic Fe. Scherrer formula was utilized to estimate the average size of nano iron particles, and the calculated result was ~ 26 nm. Also, the A-LSCFe was mechanically mixed with YSZ and the mixture was sinter at 1100 ^{o}C and analyzed by XRD in order to test the compatibility between YSZ and A-LSCFe. The curve in Figure 1 shows that only diffractions belong to YSZ and A-LSCFe could be found and no peak assigned to impurity could be detected, indicating their good chemical compatibility.

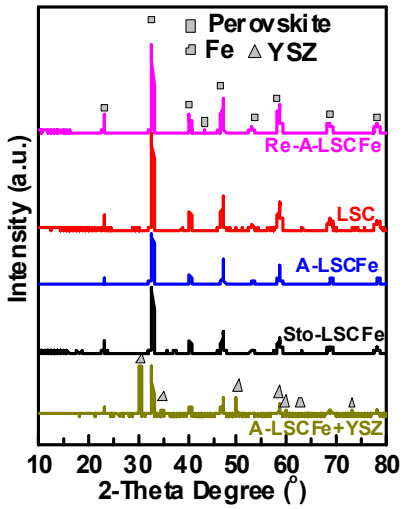

Figure 1. XRD patterns of various materials.

The H_2-TPR analysis was conducted to evaluate the influence of A-site deficiency on reducibility of Fe doped LSC materials. It can be obviously found in Figure 2 that both A-LSCFe and sto-LSCFe materials exhibited same shape and three reduction peaks from 400 °C to 800 °C could be distinguished. Specifically, the first reduction peak at around 600 °C for Sto-LSCFe can be assigned to the partial reduction of Fe^{3+} to Fe^{2+} [16] (the reduction of Fe_2O_3 to Fe_3O_4, or further to FeO) and this process is combined with the formation of certain amount of oxygen vacancies. Thermodynamically, this step is more readily to happen compared with the reduction of Fe^{3+} and Fe^{2+} to Fe directly. In comparison, this reduction peak shifts to lower temperature zone at around 560 °C for A-LACFe anode material, indicating that the reducibility of Fe in perovskite was enhanced and the creation of oxygen vacancies becomes more easily. Similarly, the higher temperature multiple reduction peaks ascribed to Fe^{2+} to Fe^0 and Fe^{3+} to Fe^0, respectively, also shifted backward by around 50 °C from 700 °C to 650 °C, while A-site deficiency was introduced. This result suggests that reduction oflin B-site to form metallic nano Fe could also be facilitated and the electrochemical performance could be further enhanced.

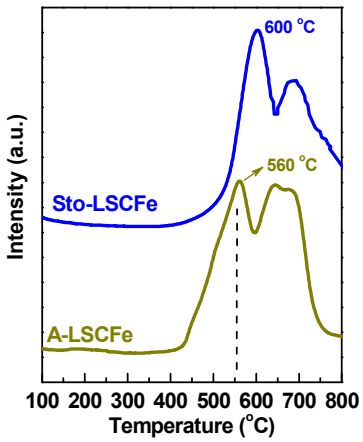

Figure 2. H_2-TPR results of sto-LSCFe and A-LSCFe materials.

The TGA analysis was conducted in 10%H_2/N_2 for the A-LSCFe and sto-LSCFe to evaluate the oxygen mobility and stability of the materials in reducing atmosphere, and the curves are shown in Figure 3. The slight mass loss at low temperature range lower than 400 °C is due to the loss of absorbed water which may happen at room temperature. The A-LSCFe started to lose weight at ~ 400 °C which is 100 °C lower than that of sto-LSCFe. The total weight loss percentage due to the formation of oxygen vacancy for A-LSCFe could reach 2.5 wt%. In comparison, the sto-LSCFe only showed the 1.8 wt% weight loss, indicating that the introduction of A-site deficiency facilitates the mobility of oxygen and promotes the formation of oxygen vacancy. After ramping up to 800 °C, the system was stabilized at 800 °C for prolonged stability test. The results shown in Figure 3 exhibit that there was no more weight change during this period, suggesting that both materials are chemical stable at our reaction condition without the further formation of oxygen vacancy. Generally, the formation of schottky vacancies consists of the loss of oxygen anion and the various kinds of valences change of B-site cations (Fe and Cr), during which the formation of metallic Fe would occure.

As the figure illustrates, both materials have no weight loss during the prolong stability test, giving the information that the formation of metallic Fe is quite fast, which happens during the ramping process and may accomplish within a short period of time.

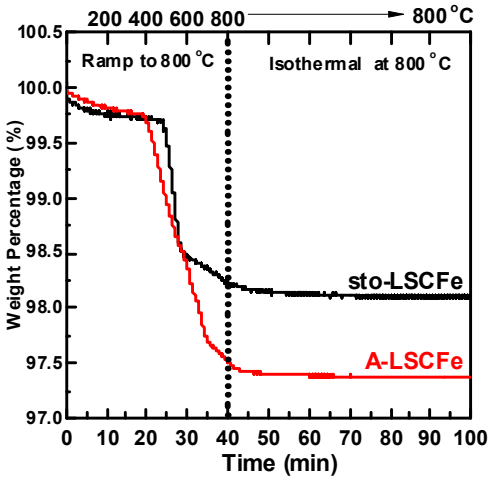

Figure 3. TGA results of sto-LSCFe and A-LSCFe materials.

The comparison of conventional and high resolution SEM images for reduced A-LSCFe and reduced sto-LSCFe are shown in Figure 4. Both samples were treated in 5%H_2-N_2 at 800 °C for 4h. The results obviously demonstrate that numerous well dispersed metallic Fe nanoparticles with uniform diameter of ~25 nm were formed on the surface of A-LSCFe. In comparison, only limited Fe particles were produced on the sto-LSCFe, even though the content of Fe in both sample was same (15%). The comparison indicates that the introduction of A-site deficiency plays a key role in the exsolution of Fe nanoparticles.

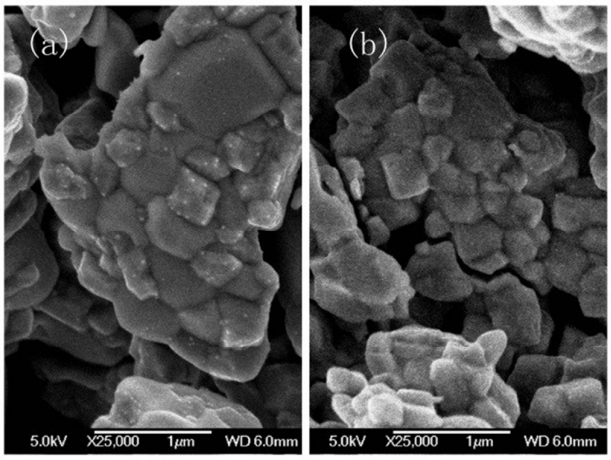

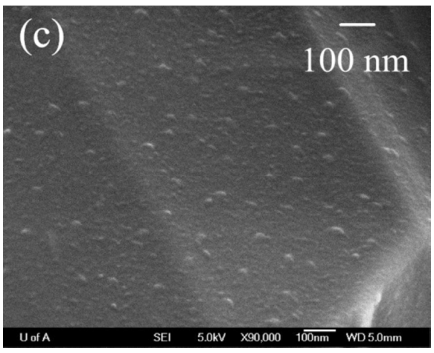

Figure 4. SEM images of reduced (a) A-LSCFe and (b) Sto-LSCFe materials and (c) high resolution SEM image of reduced A-LSCFe.

The MWCNTs were prepared by the in-situ decomposition of CH_4 at 600 °C for 4 h over pre- reduced A-LSCFe and sto-LSCFe materials mentioned above, and the SEM images of the growth of MWCNTs on each material are shown in Figures 5(a) and 5(b), respectively. The CNTs with crooked and entangled shape could be found on both materials and all had the length in the order of micro. The morphology of the MWCNTs is similar to those reported elsewhere.[17] After the reaction in CH_4 for 4h, 1.37 g CNTs were synthesized with 0.5 g A-LSCFe catalyst, compared to 0.43 g CNTs on 0.5 g sto-LSCFe catalysts. Such a difference is consistent with the results of the SEM images in Figure 5 in which less CNTs were formed over sto-LSCFe catalyst.

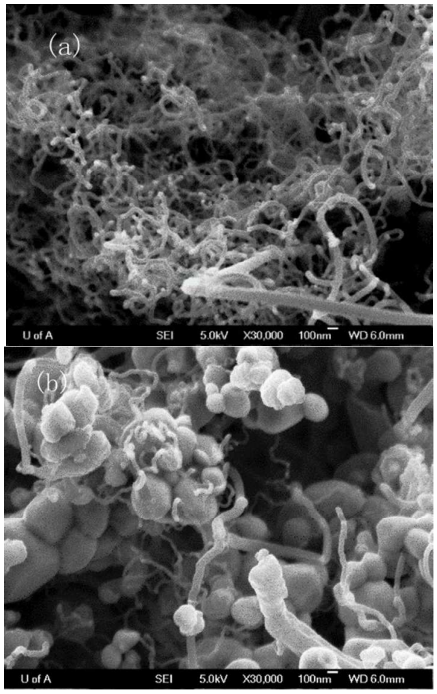

Figure 5. SEM images of MWCNTs prepared by decomposition of CH_4 at 600 °C for 4h over pre-reduced (a) A-LSCFe and (b) sto-LSCFe.

The TEM images for MWCNTs over A-LSCFe catalysts are shown in Figure 6. Figure 6a indicates that many rope structure carbon nanotubes with outer diameters ranging from 10 to 40 nm were detected. Figure 6b shows a tubular segment of MWCNTs whereas Figure 6c depicts a closer view of a ~25 nm Fe nanoparticle [indicated by EDX analysis in Figure 6c] located at the end of a MWCNT and encapsulated within the nanotube, which is consistent with a tip growth mechanism for CNTs.[18] It is worth noticing, in Figure 6d, that the growth direction of graphene layers is almost parallel to the tube axial direction. And the average spacing between two parallel layers is about 0.33 nm, which agrees well with the (002) plane lattice parameter of CNTs.

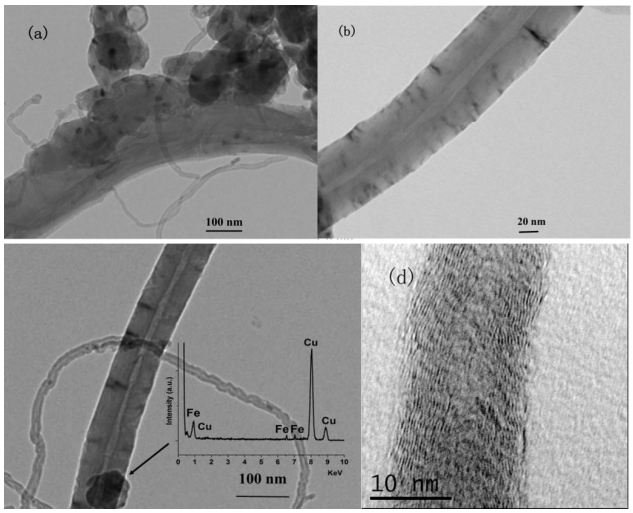

Figure 6. TEM images of (a) CNTs with different diameters, (b) segment of a CNT, (c) Fe nano particle encapsulated within a CNT as well as its corresponding EDX scan results, and (d) CNTs composed of well graphitized layers.

The I-V and power density curves (after Current-Resistance (IR) compensation) for fuel cells with various anode catalysts and temperatures in H_2 are shown in Figure 7a. The fuel cell with A-LSCFe anode can generate the maximum power density of ~430 mW cm^{-2} which is about 1.4 times the value for cell with sto-LSCFe anode. Similar performance difference could also be detected when the anode of the cell was exposed to methane. The fuel cell with A-LSCFe anode exhibited the maximum power density of around 300 mW/cm^2 At 800 °C (shown in Figure 7b), which was more than one and a half times higher than that of the cell with sto-LSCFe. The performance illustrates that the introduction of A-site deficiency into perovskite anode could significantly facilitate its electrochemical performance. The I-V and power density curves for fuel cell with A-LSCFe anode in H_2 at different temperature are shown in Figure 7c. As the temperature increased from 700 °C to 800 °C, the maximum current density and power density of the cell increased from ~380 mA cm^{-2} to 1080 mA cm^{-2} and ~210 mW cm^{-2} to ~430 mW cm^{-2}, respectively. In addition, the $La_{0.7}Sr_{0.3}CrO_3$ anode matrix impregnated with 15 mol% of $Fe(NO_3)_3$ solution (denoted as Fe/LSC) was also prepared and assembled the SOFC for electrochemical performance test. The results in Figure 7d showed that the Fe/LSC anode only exhibit the weak performance of 115 mW cm^{-2} in H_2 and 70 mW cm^{-2} in CH_4 at 800 °C, which is much worse than A-LSCFe anode.

The I-V and power density curves for the cell with A-LSCFe anode with different treatments are shown in Figure 7e. The fuel cell with A-LSCFe anode was in-situ exposed to 5% H_2/N_2 for 4h at 800 °C for the in-situ growth of nano Fe particles. After that, the temperature of the operation system was reduced to 700 °C and the fuel was switched back to pure H_2. It can be found in the figure that the in-situ exsolution of nano Fe particles promotes the electrochemical performance with the maximum power density of ~330 mW cm^{-2}, compared to the value of 210 mW cm^{-2} (shown in Figure 7c) of the cell without treatment. After that, the cells were further in-situ treated at 600 °C for 4h with CH_4 which provided carbon resource for the growth of MWCNTs. After the treatment, the fuel was switched back to pure H_2. It can be seen from the Figure 4c that the maximum powder density increased to ~460 mW cm^{-2} which was almost 1.4 times higher than that of the cell without growth of MWCNTs.

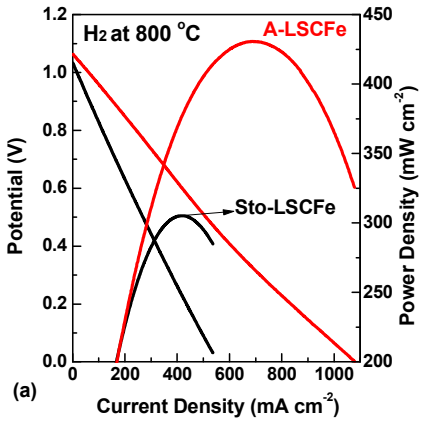

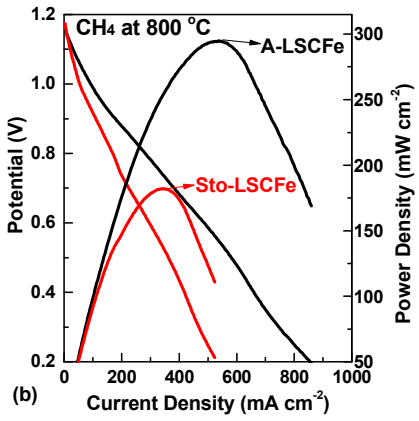

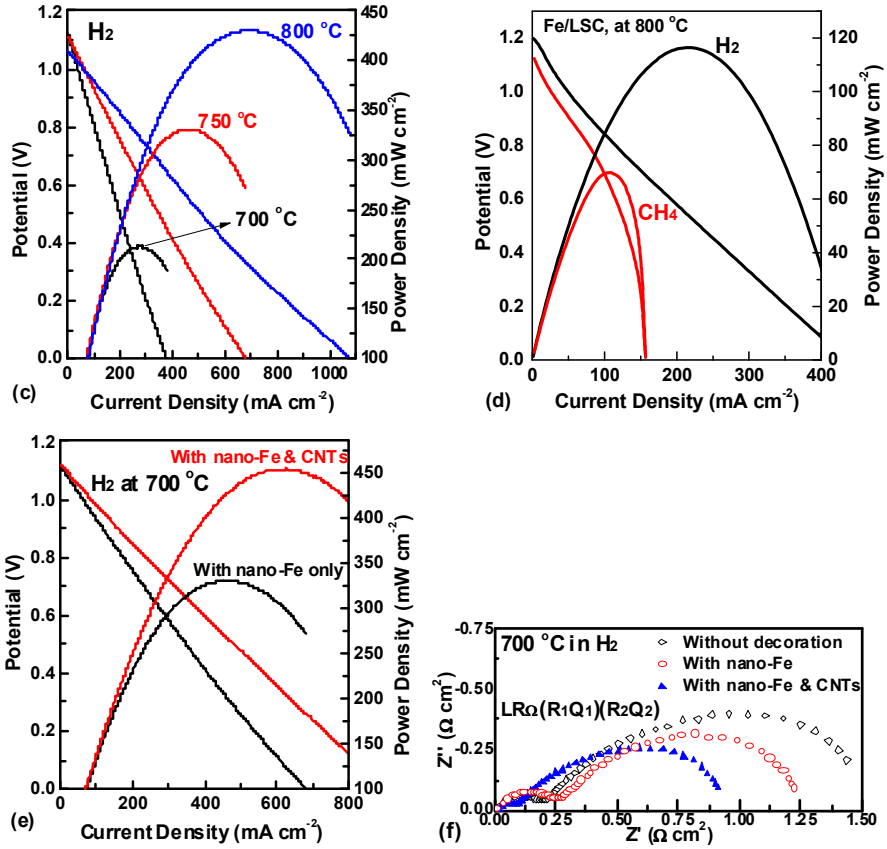

Figure 7. The I-V and power density curve of fuel cells with A-LSCFe and sto-LSCFe anodes in H_2 (a) and in CH_4 (b) at 800 °C, (c) with A-LSCFe anode fed with H_2 at different temperatures, (d) with Fe/LSC anode in H_2 and CH_4 at 800 °C, (e) with A-LSCFe anode with and without CNT in H_2 at 700 °C, and (f) the corresponding EIS of the fuel cells with different treatments.

The treatment dependence of the electrochemical properties of various composites were measured by electrochemical impedance spectroscopy (EIS) technology in H_2 atmosphere and the results are shown in Figure 7f. The best fitting results to the equivalent circuit of $LR_\Omega(R_1Q_1)(R_2Q_2)$ for all the EIS have been obtained where R_Ω represents the pure ohmic resistance. Each of the parallel circuits of resistance Ri and constant phase element Qi accounts for the respective depressed semicircle going from high to low frequencies. A parasitic inductance L was added to take into account the contribution of the equipment. This fitting result reveals that two different electrode processes (R_1 and R_2) corresponding to high and low-frequency arcs control the electrochemical reaction. The value of total activation polarization resistance (APR) can be approximately calculated taking into account the difference between the low frequency and the high-frequency intercepts on the real axis of the impedance (Z'). It can be found from the figure that the treatment exhibited no influence on ohmic resistance of the cell (~ 0.55 Ω cm^2). However, the activation polarization resistance dropped from ~1.8 Ω cm^2 to ~1.2 Ω cm^2, suggesting that the exsolution of nano iron particles (shown in SEM images) provided more active sites for the oxidation reaction of H_2.

After introducing CH_4 for 4h at 600 °C, the growth of MWCNTs could be detected. It is shown that the MWCNTs showed enhancing effect on cell performance, which results in further decrease of activation polarization from ~1.2 Ω cm^2 to ~ 0.85 Ω cm^2. Previous study in the literature ascribed the phenomenon of R_1 to charge transfer and that of R_2 to concentration polarization.[19] After the decoration of CNTs, the value of R_1 decreased from 0.35 Ω cm^2 to 0.15 Ω cm^2. Meanwhile, the value of R_2 declined from 0.85 Ω cm^2 to 0.7 Ω cm^2. Consequently, it can be speculated that the enhancing effect of CNTs is mainly due to the excellent conductivity of CNTs which facilitates the electron transportation during the reaction. The increasing charge transfer efficiency further promoted the mass transfer phenomenon.

Conclusions

In conclusion, we have developed a functional A-site deficient LSCFe perovskite material which can be utilized as anode materials for SOFCs. It can also act as the catalyst at the same time for the growth of MWCNTs. Compared to the sto-LSFC, the introduction of A-site deficiency in A-LSCFe facilitated the in-situ exsolution of iron nano particles which provided more

active sites for both the fuel oxidation reaction for SOFC and for the growth of MWCNTs. The carbon nanotubes can be produced in-situ and can promote the electrochemical performance of the cell. The superior conductivity of MWCNTs makes themselves a type of promising promoter for diverse energy storage devices.

Acknowledgements

This study was supported by the Natural Sciences and Engineering Research Council (NSERC) of the Canada Strategic Project Grant and the National Natural Science Foundation of China under grant 21303141.

References

1 H. He and J. M. Hill, *Appl. Catal. A: Gen.*, 2007, **317**, 284-292.
2 A. Atkinson, S. Barnett, R. J. Gorte, J. T. S. Irvine, A. J. McEvoy, M. Mogensen, S. C. Singhal and J. Vohs, *Nat. Mater.*, 2004, **3**, 17-27.
3 B. Huang, X. F. Ye, S. R. Wang, H. W. Nie, J. Shi, Q. Hu, J. Q. Qian, X. F. Sun and T. L. Wen, *J. Power Sources*, 2006, **162**, 1172-1181.
4 C. Liu, F. Li, L.-P. Ma and H.-M. Cheng, *Adv. Mater.*, 2010, **22**, E28-E62.
5 N. P. Brandon, S. Skinner and B. C. H. Steele, *Ann. Rev. Mater. Res.*, 2003, **33**, 183-213.
6 J. Zhang, X. Liu, R. Blume, A. Zhang, R. Schlögl and D. S. Su, *Science*, 2008, **322**, 73-77.
7 W. Zhang, P. Sherrell, A. I. Minett, J. M. Razal and J. Chen, *Energ. Environ. Sci.*, 2010, **3**, 1286-1293.
8 V. Heresanu, C. Castro, J. Cambedouzou, M. Pinault, O. Stephan, C. Reynaud, M. Mayne-L'Hermite and P. Launois, *J. Phy. Chem. C*, 2008, **112**, 7371-7378.
9 N. Halonen, K. Kordás, G. Tóth, T. Mustonen, J. Mäklin, J. Vähäkangas, P. M. Ajayan and R. Vajtai, *J. Phy. Chem. C*, 2008, **112**, 6723-6728.
10 P. Coquay, E. Flahaut, E. De Grave, A. Peigney, R. E. Vandenberghe and C. Laurent, *J. Phy. Chem. B*, 2005, **109**, 17825-17830.
11 M. H. Rümmeli, F. Schäffel, C. Kramberger, T. Gemming, A. Bachmatiuk, R. J. Kalenczuk, B. Rellinghaus, B. Büchner and T. Pichler, *J. Am. Chem. Soc.*, 2007, **129**, 15772-15773.
12 D. Takagi, Y. Homma, H. Hibino, S. Suzuki and Y. Kobayashi, *Nano Letters*, 2006, **6**, 2642-2645.
13 L. Adijanto, V. Balaji Padmanabhan, R. Kungas, R. J. Gorte and J. M. Vohs, *J. Mater. Chem.*, 2012, **22**, 11396-11402.
14 D. Neagu, G. Tsekouras, D. N. Miller, H. Menard and J. T. Irvine, *Nat. chem.*, 2013, **5**, 916-923.
15 R. Pinedo, I. Ruiz de Larramendi, D. Jimenez de Aberasturi, I. Gil de Muro, A. T. Aguayo, J. I. Ruiz de Larramendi and T. Rojo, *J. Mater. Chem.*, 2011, **21**, 10273-10276.
16 W. Gao, C. Li, H. Chen, M. Wu, S. He, M. Wei, D.G. Evans and X. Duan, *Green Chem.*, 2014, **16**, 1560-1568.
17 V. Z. Mordkovich, E. A. Dolgova, A. R. Karaeva, D. N. Kharitonov, I. A. Maslov, A. A. Kamenev and V. F. Tretjakov, *Carbon*, 2007, **45**, 62-69.
18 J. W. Snoeck, G. F. Froment and M. Fowles, *J. Catal.*, 1997, **169**, 240-249.
19 A. L. Vincent, A. R. Hanifi, J.-L. Luo, K. T. Chuang, A. R. Sanger, T. H. Etsell and P. Sarkar, *J. Power Sources*, 2012, **215**, 301-306.

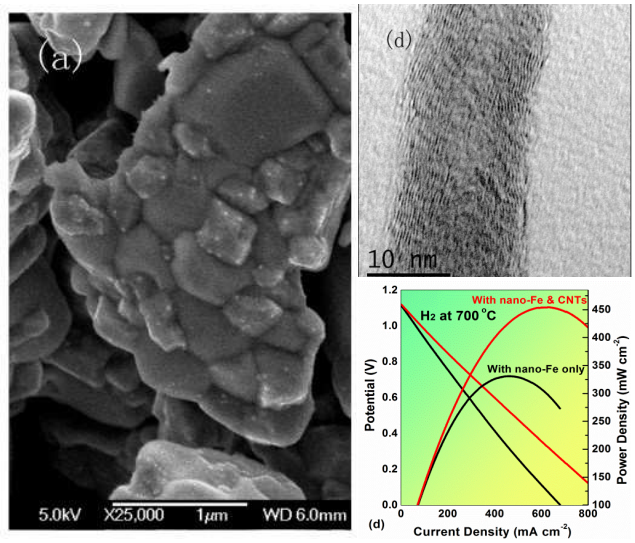

For the first time, we present a bi-functional iron-doped chromite perovskite in which the introduction of A-site deficiency significantly facilitates the in-situ exsolution of iron nanoparticles in reducing atmosphere. The material provides high-density reaction sites for both fuel oxidation in SOFCs and growth of carbon nanotubes which further enhances the electrochemical performance of SOFCs.